Pure Appl. Geophys. 181 (2024), 3409–3429

https://doi.org/10.1007/s00024-024-03611-z

Pure and Applied Geophysics

Modeling the Ventilation of the Vortex Periphery for Anticyclonic Quasi-Permanent Lofoten Vortex

E. V. Novoselova,[1,2] P. A. Fayman,[3] A. A. Didov,[1,3] M. V. Budyansky,[1,3] I. S. Solonets,[3] T. V. Belonenko,[1] and M. Yu. Uleysky[3]

Abstract—This study examines the structure of the Lofoten Anticyclone, located in the Lofoten Basin of the Norwegian Sea. The high-resolution ROMS model is used for hydrodynamic modeling of the Lofoten Basin circulation. The dynamics of the Lofoten Vortex are investigated using the Lagrangian methods, where trajectories of passive tracers advected by the model velocity field are calculated, and Lagrangian indicators are computed for the studied region. Lagrangian markers initially located both in the core and on the periphery of the Lofoten Vortex are considered, showing different behaviors. Lagrangian markers in the core move along closed trajectories with angular velocities depending on their distance from the eddy's center. Those initially on the periphery form a series of *S*-shaped folds and twists, entering and exiting the eddy. We refer to this process as "ventilation of the vortex periphery". We demonstrated that particles leave the core and periphery of the eddy intermittently rather than uniformly over time, and the statistics of this process are analyzed. Additionally, it was found that the center of the Lofoten Vortex not only drifts cyclonically at an average speed of 3.8 cm/s but also oscillates in the horizontal plane, with the amplitude increasing in the eastern part of the Vortex's movement area.

Keywords: Lagrangian modeling, ROMS, Lofoten vortex, Norwegian Sea, Lagrangian indicators, Lagrangian markers.

1. Introduction

The Lofoten Basin in the Norwegian Sea is one of the most dynamically active regions of the World Ocean, characterized by local peaks of kinetic energy of synoptic (mesoscale) eddies. In the work of Volkov et al. (2013), this region is called a "hotspot" of the Northern seas, as satellite altimetry data indicate the presence of a local maximum in sea level variance here. The Lofoten Basin, a transit zone for warm and salty Atlantic water masses heading towards the Arctic Ocean, plays a key role in sustaining the global meridional circulation. In this region, Atlantic waters release heat into the atmosphere and mix with surrounding waters, which is crucial for the subsequent formation of deep waters in the neighboring Greenland Sea. The Lofoten Basin is a topographically isolated feature with almost circular closed isobaths and a maximum depth in the center reaching 3250 m. It is bounded by the Mona Ridge to the northwest, the Scandinavian Peninsula to the east, the Helgeland Ridge to the southwest, and the Vøring Plateau to the south (Fig. 1). Despite its subpolar location, there is virtually no inflow of Arctic waters into the basin (Belonenko et al., 2021a, 2021b; Blindheim & Østerhus, 2013). The thermohaline structure of the Lofoten Basin's waters is shaped under the influence of Atlantic waters. Relatively warm and saline Atlantic waters are transported into the basin by the Norwegian Atlantic Slope Current (NwASC), the Norwegian Coastal Current (NCC), and the Norwegian Atlantic Front Current (NwAFC) (Fig. 1).

The topographic isolation, seabed relief, and barotropic and baroclinic instability of the branches of the Norwegian Current create exceptionally favorable conditions for the formation of mesoscale eddies in the basin. In the deep-water part of the basin, there is a quasi-permanent anticyclonic Lofoten Vortex (LV), whose stability is enhanced by the

Supplementary Information The online version contains supplementary material available at https://doi.org/10.1007/s00024-024-03611-z.

[1] Saint Petersburg State University, Saint Petersburg 199034, Russia. E-mail: novoselovaa.elena@gmail.com

[2] Nansen International Environmental and Remote Sensing Center Scientific Foundation, Saint Petersburg 199034, Russia.

[3] Il'ichev Pacific Oceanological Institute, Vladivostok 690041, Russia.

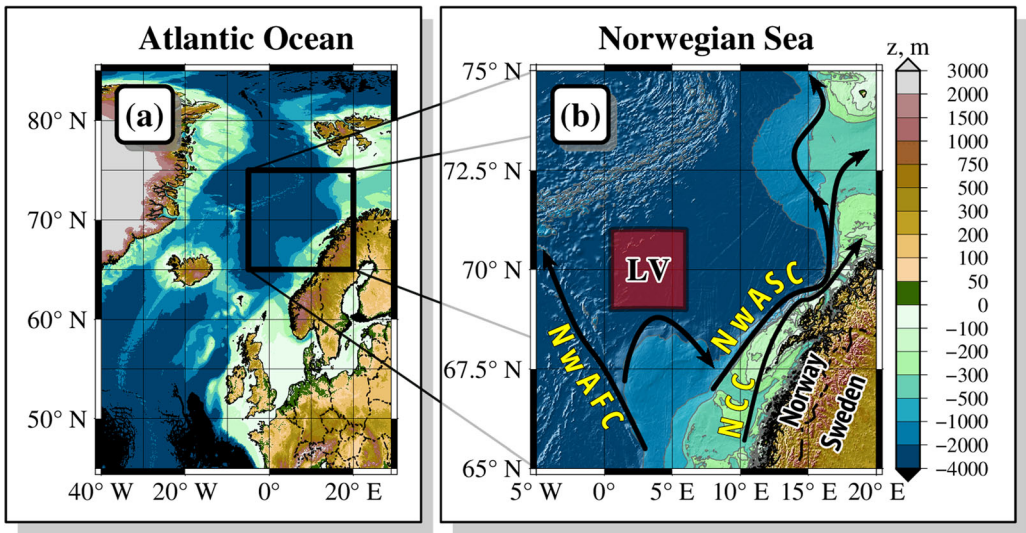

Figure 1
a The study area. The color shows the bottom topography (m). **b** The arrows show the main currents: *NwASC* Norwegian Atlantic Slope Current, *NCC* Norwegian Coastal Current, and *NwAFC* Norwegian Atlantic Frontal Current. The letters LV show the location of the Lofoten Vortex

specific features of the seabed topography (Belonenko et al., 2021a, 2021b; Santeva et al., 2021; Volkov et al., 2015).

In modern oceanography, there are two main approaches to studying mesoscale eddies. In the first approach, the eddy is treated as a three-dimensional structure ("a bag of water"), with its properties examined using CTD profiling data, gliders, and ARGO buoys, as well as through 3D hydrodynamic modeling. In the second approach, eddies are analyzed using satellite imagery or two-dimensional fields of various Eulerian and Lagrangian hydrodynamic characteristics. In this approach, the eddy is represented as a closed contour or area bounded by an isoline of some Eulerian or Lagrangian characteristic.

Mesoscale eddies play a crucial role in oceanic circulation, characterized by their dynamics where nonlinear effects are predominant. Here are some definitions of mesoscale eddies:

1. Stewart (2006) defines mesoscale eddies as "turbulent or spinning flows on scales of a few hundred kilometers".
2. Zhmur (2011) describes a mesoscale eddy as a rotating core ("a bag of water") with surrounding water masses rotating in the same direction as the core's fluid particles.
3. Cushman-Roisin (1994) offers another definition: An eddy is "a closed circulation that is relatively persistent. By persistency, we mean that the turnaround time of a fluid parcel embedded in the structure is shorter than the time during which the structure remains identifiable".

Today, the Lofoten Vortex (LV) attracts significant interest from researchers, serving as a unique natural laboratory for studying vortex structures in the ocean. It consists of a lens of warm salty water at depths of 300–1000 m, with a horizontal scale of about 60–80 km. The radius of the vortex core, according to glider data, is 18 ± 4 km (Yu et al., 2017). The existence of a quasi-permanent anticyclone in the basin is confirmed by in situ measurements, satellite data, and results from hydrodynamic modeling. The work by Belonenko et al. (2014) indicates its most likely location within the coordinates of 69°–70° N and 2°–5° E. The large eddy is in constant motion, primarily along the isobath, moving in a cyclonic direction at a speed of 3–4 cm/s relative to the center of the basin (Yu et al., 2017). Maximum orbital speeds within the vortex can

reach 50–70 cm/s. Even without external energy input, the vortex in this area can maintain between 60 and 90% of its core volume (Trodahl et al., 2020, and references herein). Continuous rejuvenation of the vortex, both through convection and through merging with other vortices that contribute to an increase in potential vorticity, is also necessary for maintaining the stability of the large vortex in an aggressive environment with high deformation rates (Novoselova, 2022; Travkin & Belonenko, 2021; Zhmur et al., 2022, 2023). The stability of the large vortex is ensured by maintaining high anticyclonic vorticity through merging with other anticyclones formed as a result of baroclinic instability of the branches of the Norwegian current (see review in Fedorov et al., 2021), as well as due to winter convection (see review in Koldunov & Belonenko, 2020).

We consider the large vortex as a rotating structure consisting of a core and the surrounding water, referred to as the vortex periphery. The periphery of the vortex rotates along with its core; however, unlike the core, the periphery exchanges particles intensively with the background waters (Ryzhov & Koshel', 2011) The renewal of the water in the vortex core occurs much less frequently and is associated with "catastrophic" events for the vortex, such as winter convection or the merging of the large vortex with another anticyclone (Novoselova, 2022; Trodahl et al., 2020).

The dynamics and thermohaline properties of the LV have been repeatedly studied by various authors (see, for example, Volkov et al., 2013, 2015; Yu et al., 2017; Trodahl et al., 2020; Novoselova, 2022; Travkin & Belonenko, 2021; Zhmur et al., 2022, and references herein). The research was carried out using satellite, field, and model data. Studies have also been conducted using the regional high-resolution oceanic model ROMS, for example, in Trodahl et al. (2020) the vortex dynamics of the Lofoten basin is investigated using this model. The authors consider the regeneration of the LV due to repeated events of the LV fusion with other anticyclones and show that the core waters are gradually replaced by other waters, however, the LV can still be identified as a stable extreme of negative potential vorticity.

In this paper, we follow a different path and show that the mechanism of vortex water renewal due to the fusion of anticyclones is not the only one, and the advection of vortex particles is not limited to the simple fusion of two or more vortices and has a much

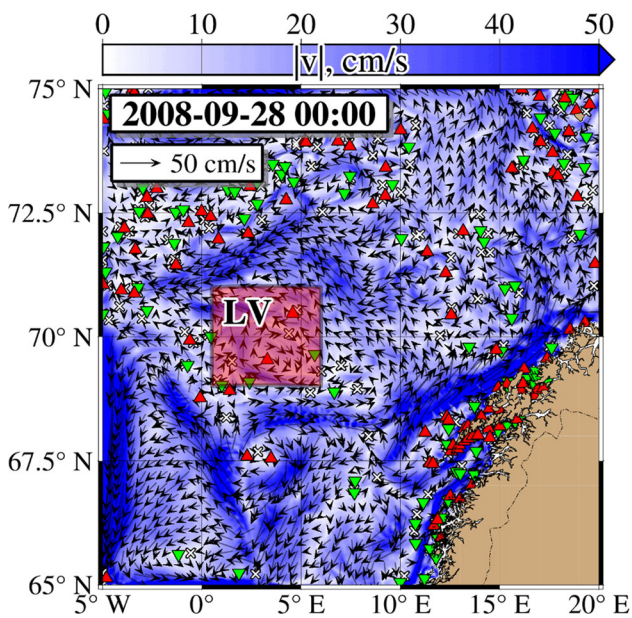

Figure 2
Current velocity in the Lofoten Basin (m/s) calculated using the ROMS model at 00:00 on September 28, 2008. The area of the Lofoten vortex location is highlighted with a rectangle

more complex and subtle nature. To prove this statement, we perform Lagrangian modeling. It is important to note that in this study we consider the 2D advection of waters near the vortex, the 3D model of which we obtained based on the ROMS model. To study the 2D advection of waters, we selected two horizons at depths of 50 and 400 m.

In this paper, we will try to answer the following questions: (i) How do water particles leave the core and periphery of the LV, being replaced by particles from the background environment of the vortex? (ii) Does this process, called core water ventilation (or "ventilation of eddy periphery"), occur uniformly or in portions? (iii) Do other vortices and hyperbolic points located in the vicinity of the LV affect this process? (iv) What are the statistics of the time of particles removal from the LV core and periphery into the background stream? (v) How does the trajectory of the LV center change? The answers to these and other questions constitute the purpose of the study.

2. Model Description

The study utilizes the *Regional Ocean Modeling System (ROMS)*, which is a system of differential nonlinear equations governing fluid motion with a free surface, employing an s-coordinate system that adapts to the seabed topography (Shchepetkin & McWilliams, 2005). The modeling area lies within the latitudinal range of 65° N–75° N and the longitudinal range of 5° W–20° E. The horizontal grid resolution is 1.5 km, while the vertical structure consists of 64 s-layers, providing optimal resolution for surface and bottom layers (Shchepetkin, 2003).

The global digital elevation model ETOPO2, developed by the National Geophysical Data Center (NGDC) in 2006, was used to create the depth array. ETOPO2 is a 2 arc-minute grid containing elevation and bathymetry data for the entire world. The direction and speed of the surface wind were obtained from the Daily ASCAT global wind field with a spatial resolution of 0.25° (Bentamy & Croize Fillon, 2012). Atmospheric data, including pressure, incoming shortwave radiation, relative humidity, air temperature, precipitation, and cloud cover, were taken from the NCEP-DOE AMIP-II atmospheric analysis (Kanamitsu et al., 2002). Daily sea surface temperature fields were obtained from the Operational Sea Surface Temperature and Sea Ice Analysis (OSTIA) used for heat flux correction (Good et al., 2020). The monthly climatological sea surface salinity was taken from the World Ocean Atlas 2018 and used for freshwater flux correction (Zweng et al., 2018). Data on temperature, salinity, sea level, and currents for establishing initial conditions and conditions at the liquid boundary were obtained from the GLORYS12V1 oceanographic reanalysis (Lellouche et al., 2018). Dirichlet boundary conditions were applied to all open boundaries for the three-dimensional fields of temperature, salinity, and velocity components.

The modeling start date is January 1, 2008. The first six months serve as a period for ramp-up and adaptation of the model's initial conditions. The main working period was from mid-August to mid-October 2008 when the LV was observed clearly in the study area. The simulation results were recorded every three hours of model time.

The surface current field calculated by the ROMS model for September 28, 2008, is presented in Fig. 2. The branches of the Norwegian Slope Current and Coastal Current, extending along the coasts of Scandinavia with speeds exceeding 50 cm/s, are visible. Additionally, a branch of the Norwegian Front Current with lower speeds can be seen along the Helgeland Ridge. In the western part of the region, the LV center is located at the point of 69.5° N and 3.2° E.

3. Verification

Verification of the ROMS simulation results was performed using CTD measurements and AVISO satellite altimetry data. CTD measurement data were used for diagnostic calculations to obtain estimates of the three-dimensional structure of the LV. AVISO satellite altimetry data allow us to obtain the structure

of the LV on the surface. Data from the GLORYS12V1 oceanic reanalysis, available on the Copernicus Marine Environment Monitoring Service (CMEMS) portal, were also used to verify the simulation results (http://marine.copernicus.eu) (Table 1).

3.1. *Verification Based on the Results of Diagnostic Calculations*

A linear diagnostic model was used for diagnostic calculations, the theoretical foundations of which are formulated in the work of Sarkisyan (1977). The initial system of formulas includes simplified equations of motion (advection and horizontal turbulent exchange are excluded) and continuity in the approximations of hydrostatics and Boussinesq. Wind friction stress and a "rigid lid" were set as boundary conditions on the sea surface, and a no-slip condition was set at the bottom. After converting the original formulas, the resulting system of partial differential equations includes the elliptical sea level equation, the continuity equation, and explicit formulas for calculating the horizontal components of the flow vectors. The numerical solution of the elliptical sea level equation uses the method described in the monograph by Kochergin (1978). Its essence lies in reducing the Neumann problem to the Dirichlet problem, i.e. the level surface is calculated by successive approximations at the nodes of the closed boundary of the computational domain, and then at the inner points of the domain. When numerically approximating the second derivatives by horizontal coordinates, a scheme of central differences is used, and when approximating the first derivatives, a scheme of directional differences is used. Successive approximations of the resulting system of linear equations for the level values at the grid nodes are performed using the Gauss–Seidel method. Central differences were used to discretize the equations of the horizontal components of the velocity vector. Subsequently, the complete system of numerical equations of the model was solved by the iterative method until it was fully established. The difference between the proposed model and the Sarkisian D1 linear diagnostic model lies in a more correct numerical scheme for solving the boundary value problem for the level. This allows the method of successive approximations to coordinate the field of currents with the bottom relief and shoreline. The second feature of the model is the exclusion of the overestimated influence of sharp bottom relief gradients. Such a model has been successfully used to calculate currents based on CTD measurements (Fayman & Ponomarev, 2018) and climate data (Fayman, 2015).

The input data of the diagnostic model are the depth, the wind field in the driving layer of the atmosphere, and the three-dimensional field of water density (or temperature and salinity of water) on a horizontally uniform grid. The fields of temperature and salinity of water were taken from the results of CTD measurements conducted by the Arctic and Antarctic Research Institute aboard the NIS "Professor Wiese" during three expeditions: September 5–9, 1987, September 10–18, 1989 and September 4–12, 1990. The station diagrams are shown in Fig. 11 (Appendix). The data of CTD measurements performed in the above-mentioned expeditions are publicly available in the World Ocean Database 2018 (WOD18) (Boyer et al., 2018). This data is available up to a depth of 1100 m. Data on the temperature and salinity of seawater at depths of more than 1100 m were taken from the World Ocean Atlas 2023 database (Reagan et al., 2024). Data at depths from 1100 to 1500 m were taken from the data averaged for September, and at depths over 1500 m—from data averaged over the summer period (July, August, September). The modeling area was taken within 0.5°–6.5° E, 69°–71° N for calculations based on the results of the 1987 expedition and within 0.5°–6.5° E, 68.5°–71.5° N for calculations based on the results of the expeditions in 1989 and 1990. The horizontal grid pitch is 0.05°. The depth field was taken from the global relief model 2-minute Gridded Global Relief Data (ETOPO2) v2 (NOAA National Geophysical Data Center, 2006). The data of sea temperature and salinity were interpolated onto the regular grid using the ordinary kriging method. The scheme, coordinates, and dates of the CTD stations in the expeditions of September 1987, 1989, and 1990 are presented in the Fig. 11 and Table 1 in the Appendix.

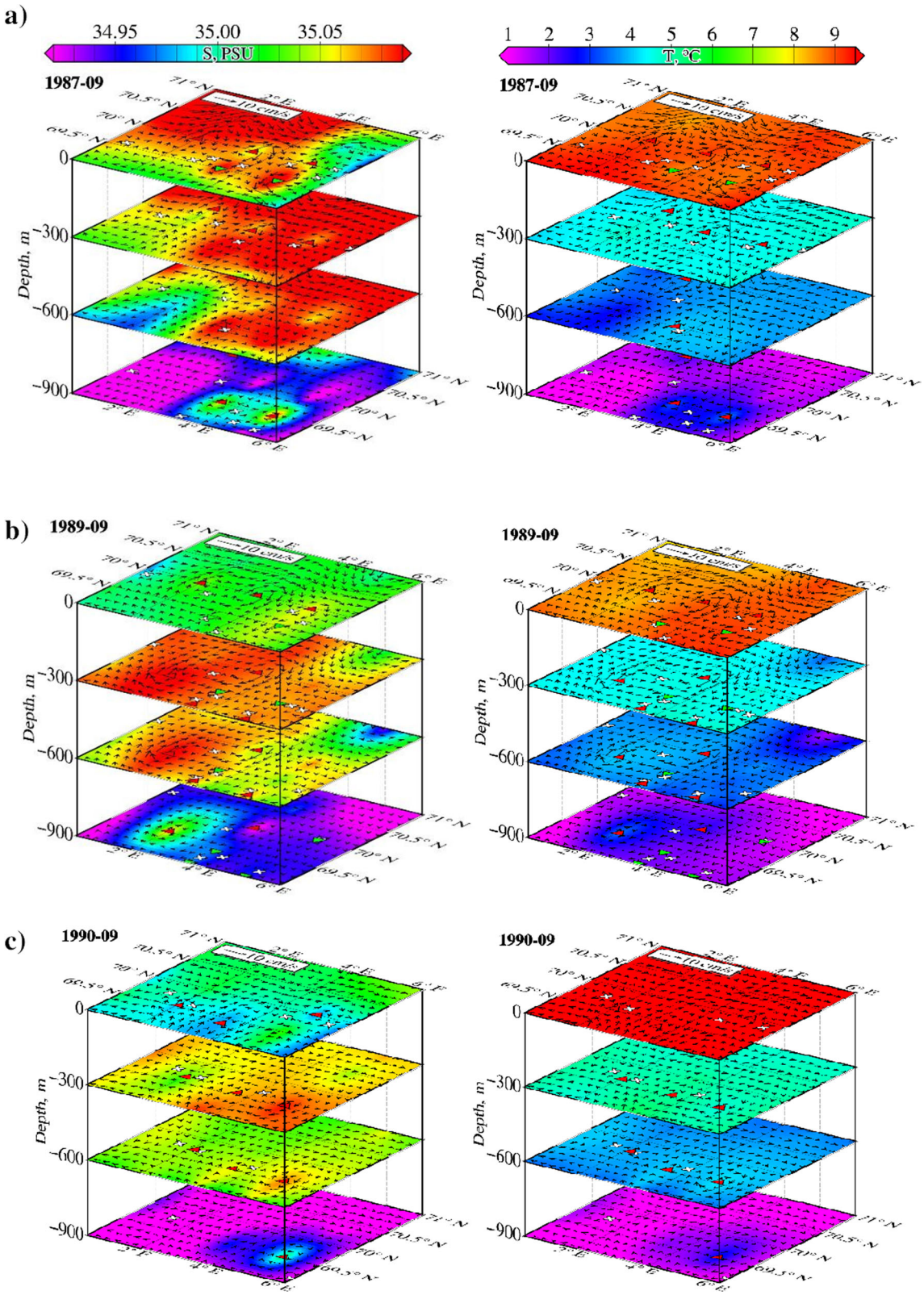
a)
34.95
35.00
35.05
S, PSU
1 2 3 4 5 6 7 8 9
T, °C
1987-09
1987-09
b)
1989-09
1989-09
c)
1990-09
1990-09
Depth, m
0
-300
-600
-900
10 cm/s

◀Figure 3
The results of diagnostic calculations based on the results of the expeditions in September 1987 (**a**), 1989 (**b**), and 1990 (**c**)

The results of the expedition in September 1987 showed the following. An anticyclonic vortex with a diameter of 100 km is observed in the northwestern part of the calculated region and is traced in the upper kilometer layer. A more extensive anticyclonic circulation, with a diameter of up to 200 km, is observed in the southeastern part of the calculated area and is traced at depths from 300 to 900 m (Fig. 3a).

The results of the expedition in September 1989 showed that an anticyclonic vortex with a diameter of 200 km is observed throughout the calculated area in the upper kilometer layer. At the periphery of the anticyclonic vortex, cyclonic vortices with a diameter of up to 50 km are observed in the upper 400-m layer (Fig. 3b). The two-core structure of the anticyclonic vortex, which is well traced below 500 m, is associated with errors in two-dimensional interpolation, which in turn is associated with a small number of CTD stations.

According to the results of the September 1990 expedition, the anticyclonic vortex is located in the southeastern part of the calculated region and is traced in the upper kilometer layer (Fig. 3c).

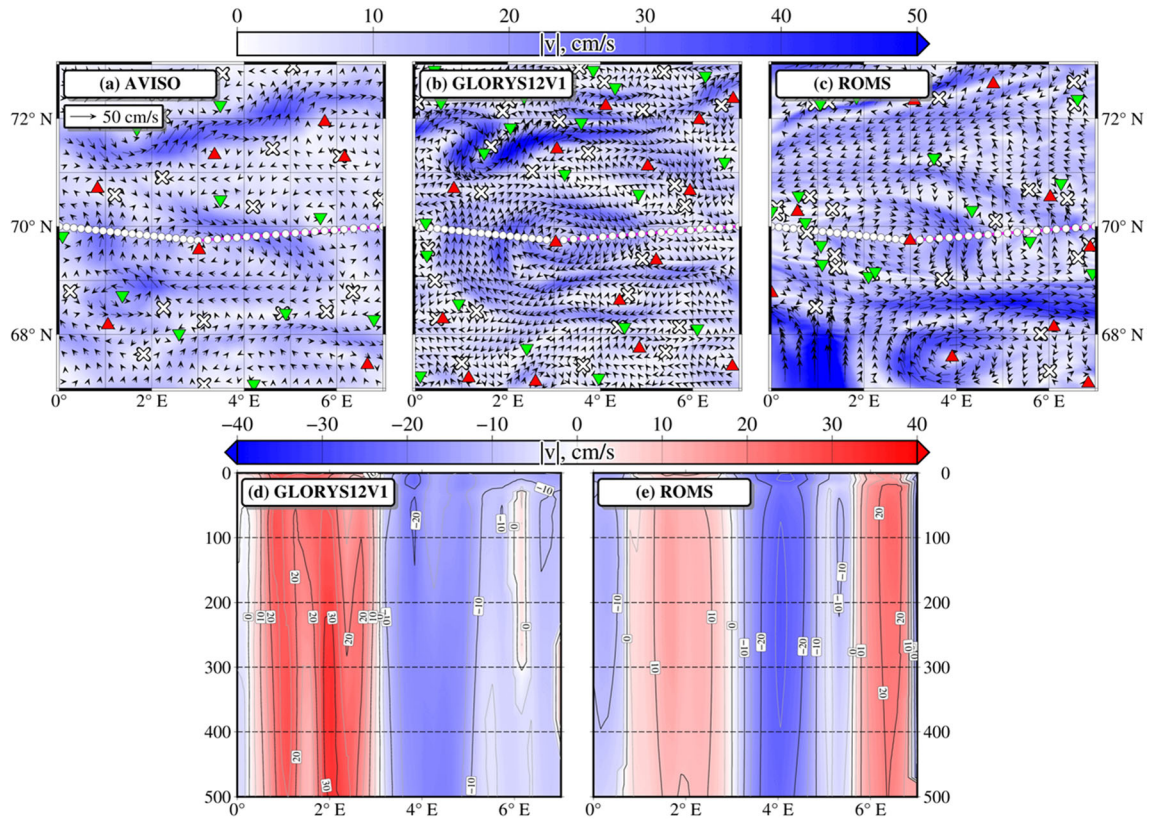

Figure 4
Current velocity based on AVISO (**a**); the layer of 200 m based on GLORYS12V1 (NEMO) (**b**), the same based on ROMS (**c**) on September 16, 2008 at 12:00. The arrows indicate the current velocity vectors. The white dotted line shows the zonal section through the Lofoten Vortex. The red triangles indicate the centers of anticyclones, and the green ones indicate the centers of cyclones. Crosses indicate hyperbolic points. The corresponding flow velocities in the vertical zonal section through the center of the Lofoten Vortex are based on GLORYS12V1 (NEMO) (**d**) and ROMS (**e**)

The expeditions of 1987 and 1990 were conducted in early September and have common features. The materials of both expeditions revealed that an intensive anticyclonic vortex with a diameter of up to 200 km is located in the southeastern part of both of them. A smaller anticyclonic vortex is located on the northwestern periphery of this anticyclone. The 1989 expedition was conducted in mid-September and shows an anticyclonic vortex in the central part of the calculated area with pronounced cyclonic vortices on the periphery. This is in good agreement with the simulation results obtained based on ROMS.

3.2. *Verification Based on AVISO Satellite Altimetry Data and Reanalysis GLORYS12V1*

AVISO data—dynamic topography measurements (ADT, Absolute Dynamic Topography)—are the result of combining measurements from all altimetric missions, including the TOPEX/Poseidon and ERS series satellites, from 1993 to the present. The spatial resolution of the data is 0.25° latitude and longitude, and the time discreteness is 1 day. The latest update of the array includes new sensor and atmospheric corrections, new calibration of various altimeters, and a new tidal model, and also takes into account a longer base period of 20 years to estimate average sea level (Pujol et al., 2016). Sea level anomalies were calculated relative to the mean sea level [Mean Sea Surface, MS], available on the Aviso portal + (http://www.aviso.altimetry.fr/en/data/products/auxiliary-products/mss.html).

GLORYS12V1 (Global Ocean Physics Analysis) is a global vortex-resolving reanalysis of the World Ocean with a spatial resolution of 1/12° at 50 vertical levels for the period when altimetric observations are available. It is based on the CMEMS global real-time forecasting system. The hydrodynamic model of ocean circulation NEMO (Nucleus for European Modeling of the Ocean) is the basis of the analysis. Observations are assimilated using a low-order Kalman filter. In situ data from satellite altimeters, sea surface temperature, sea ice cohesion, and vertical profiles of water temperature and salinity are assimilated together.

We calculated the 3D dynamic and thermohaline characteristics for the study area using the ROMS model and compared them with the corresponding characteristics from the GLORYS12V1 (NEMO) reanalysis. Figure 4 shows a comparison of velocities at a horizon of 200 m and a vertical section through the vortex center. Stationary points in the velocity field on a given date are marked on maps with triangles and crosses. Elliptical stationary points, shown as triangles and located in the centers of vortices, are points around which the movement is stable and circular. Hyperbolic stationary points, shown as crosses, are located between vortices and are unstable, with two directions in which the waters converge to such a point, and two others in which they diverge (Prants, 2014; Prants et al., 2017). The trajectories of liquid particles and stationary points in the velocity field may acquire or lose hyperbolicity over time. This means, in particular, that hyperbolic stationary points can appear and disappear over time. Hyperbolic points characterizing instability can significantly affect neighboring areas of the water.

It can be seen from the figures that the structures of the LV, obtained from velocity data from different data sets, are consistent with each other. The center of the LV on the maps (Fig. 4a–c) coincides and has coordinates 69.7° N, 3.2° E. At the same time, it should be noted that the location of the centers of other mesoscale vortices differs on different maps. These features are explained by the different spatial resolution of the datasets: 1/4° for AVISO, 1.5 km for ROMS, and 1/12° latitude and longitude for GLORYS12V1 (NEMO), which corresponds to 3.2 km in latitude and 9.3 km in longitude. It is important to note that there are several cyclones on the periphery of the LV, as well as hyperbolic points shown by crosses, which are fixed for both data sets. Cyclones surround the LV from all sides, forming a so-called shield. Carton (2001) calls such anticyclones, surrounded by a ring with relative vorticity of the opposite sign, "shielded vortices". A similar structure of an anticyclonic vortex surrounded by smaller-scale cyclonic vortices was apparently first observed by Kennelly et al. (1985) on the periphery of ring 82B in the Atlantic Ocean. The shielded mechanism of their formation was confirmed in numerical calculations by Sokolovskiy (1988). However, in addition to the cyclones indicated in Fig. 4 by green triangles, hyperbolic points are also observed on the periphery

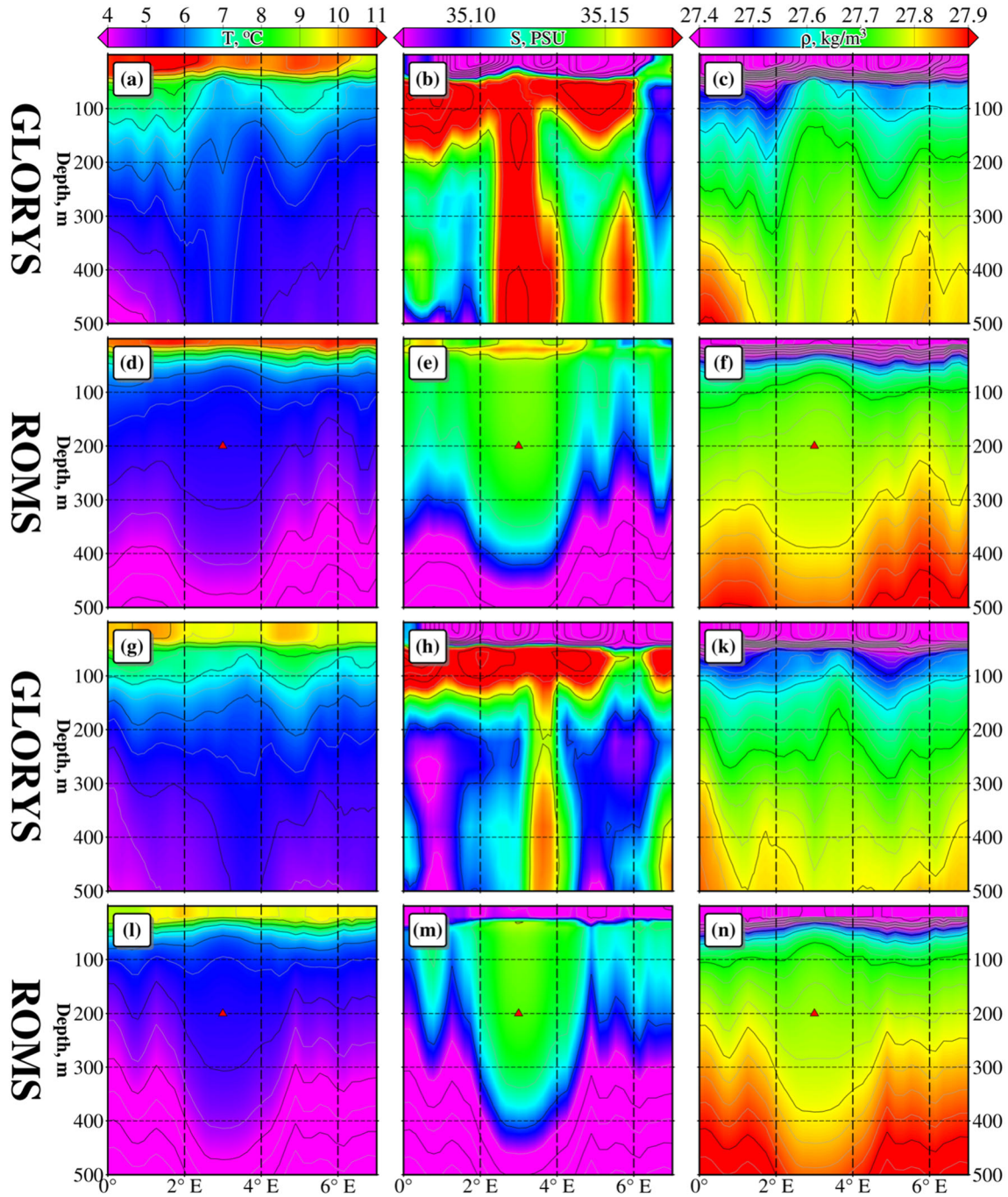

Figure 5

Distributions of temperature, salinity, and potential density according to GLORYS12V1 (NEMO) and ROMS data on September 16 (**a**–**f**) and September 27 (**g**–**n**), 2008. Zonal sections are constructed through the center of the Lofoten Vortex. The red triangles show the center of the Lofoten Vortex at a depth of 200 m

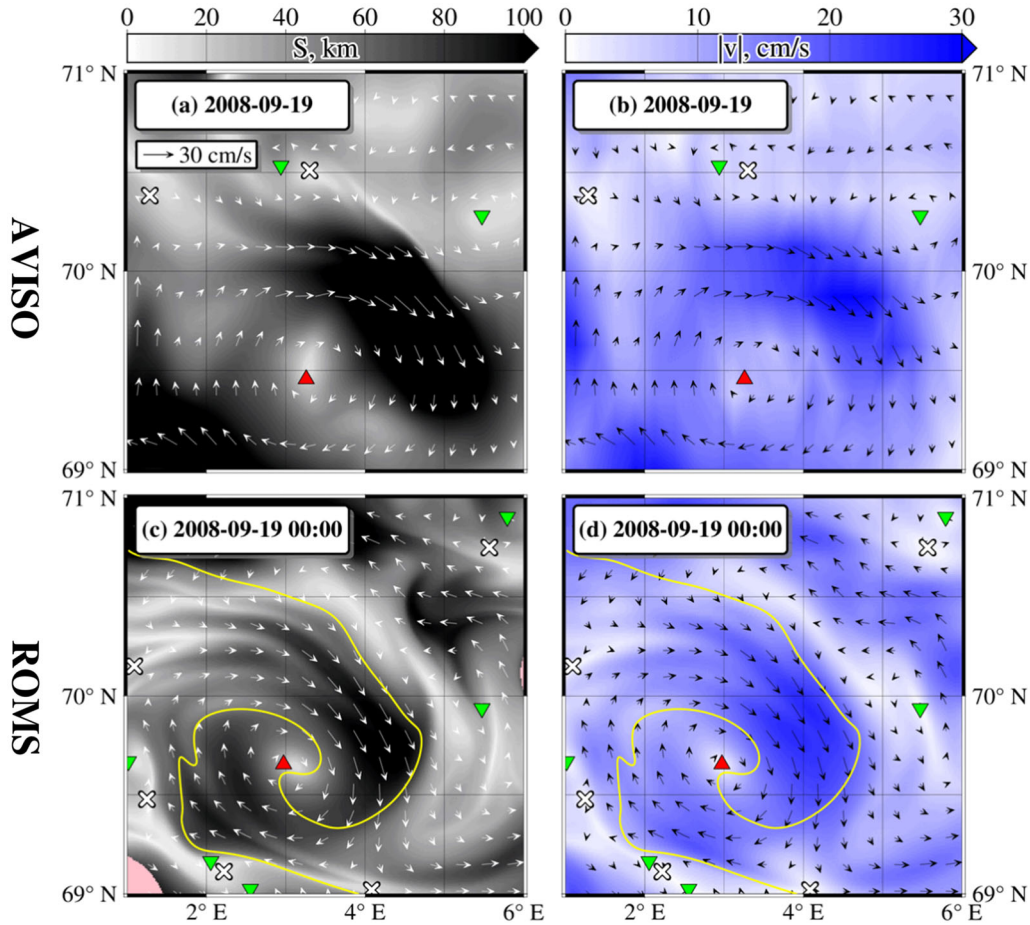

Figure 6

Maps of trajectory lengths accumulated over the previous 5 days from the dates indicated in each of the slides, according to AVISO (**a**) and ROMS (layer of 400 m) (**c**). Corresponding fields of flow velocities are presented in slides (**b**) and (**d**). The length of the trajectories and the magnitude of the flow velocity are shown in color and correspond to the scales. The red triangle indicates the center of anticyclonic Lofoten Vortex, and the green triangles indicate the centers of cyclones. The crosses indicate hyperbolic points. The yellow line is a fragment of the marker spot evolution ("Experiment with a Segment")

of the LV, the influence of which on the dynamics we will consider below.

A comparison of velocity fields constructed using NEMO (GLORYS12V1 reanalysis) and ROMS models with velocities constructed using AVISO (Fig. 4) shows that although velocity distributions have spatial differences, the center of the LV has the same coordinates in all three data sets. However, there are fewer vortices and hyperbolic points in the AVISO velocity fields, which is obviously due to the coarser spatial resolution of the grid in AVISO.

A comparison of vertical sections of thermohaline characteristics according to ROMS and GLORYS12V1 (NEMO) is shown in Fig. 5. The comparison shows that the LV lens is brighter and better stratified according to ROMS data than according to GLORYS12V1. During the period under review (September–October), the LV has the characteristic shape of a biconvex anticyclonic lens. The distributions in Figs. 5 are not fundamentally different from each other. The upper layer (above the LV core) is stably stratified in temperature and unsteadily

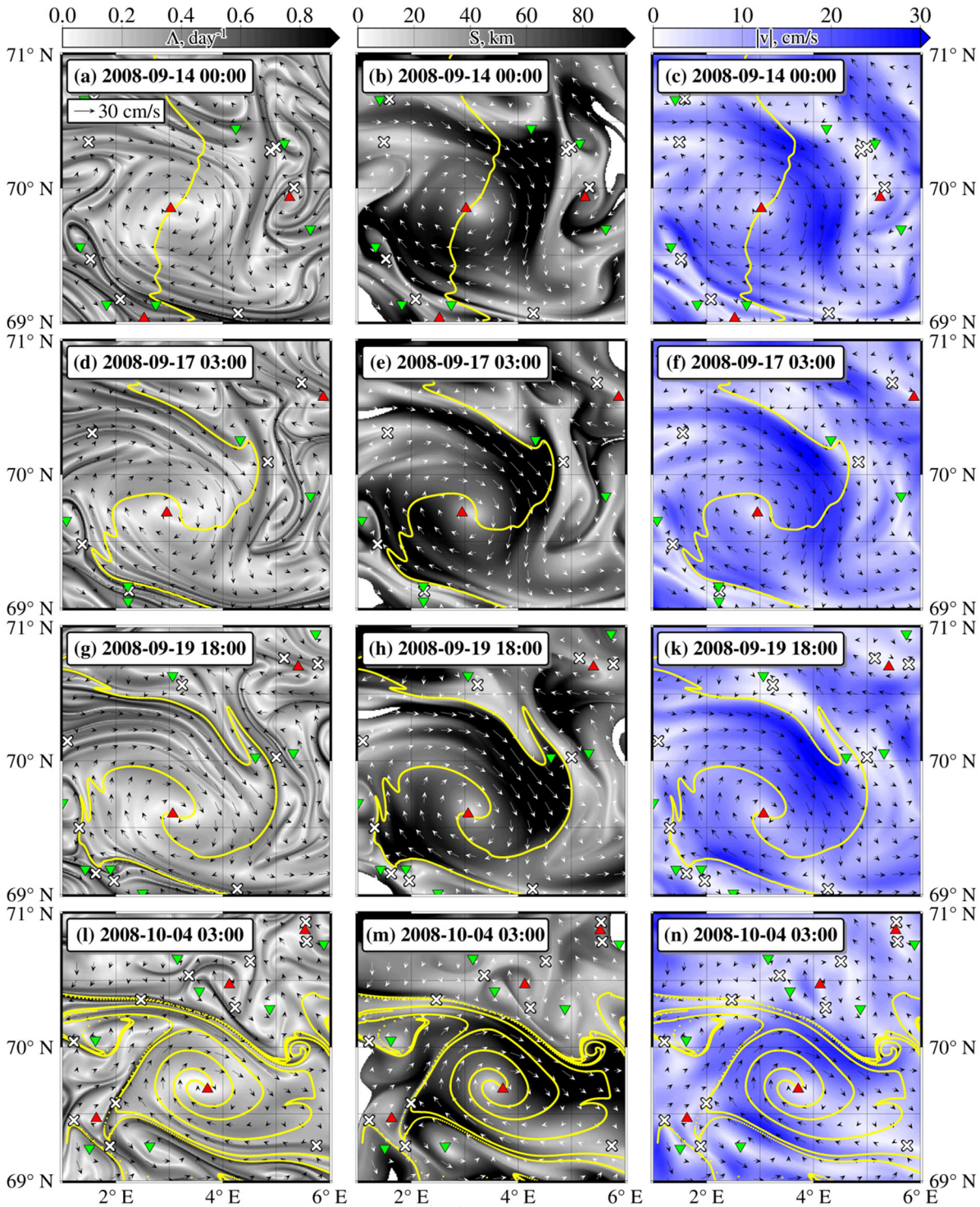

◀Figure 7

Individual slides "Experiment with a Segment": the evolution of the Segment against the background of the Lofoten Vortex: Λ-maps (left column), *S*-maps (central column), and the velocity field (right column) for a layer of 50 m according to ROMS data. The red triangles indicate the centers of anticyclones, and the green ones indicate cyclones. The crosses indicate hyperbolic points

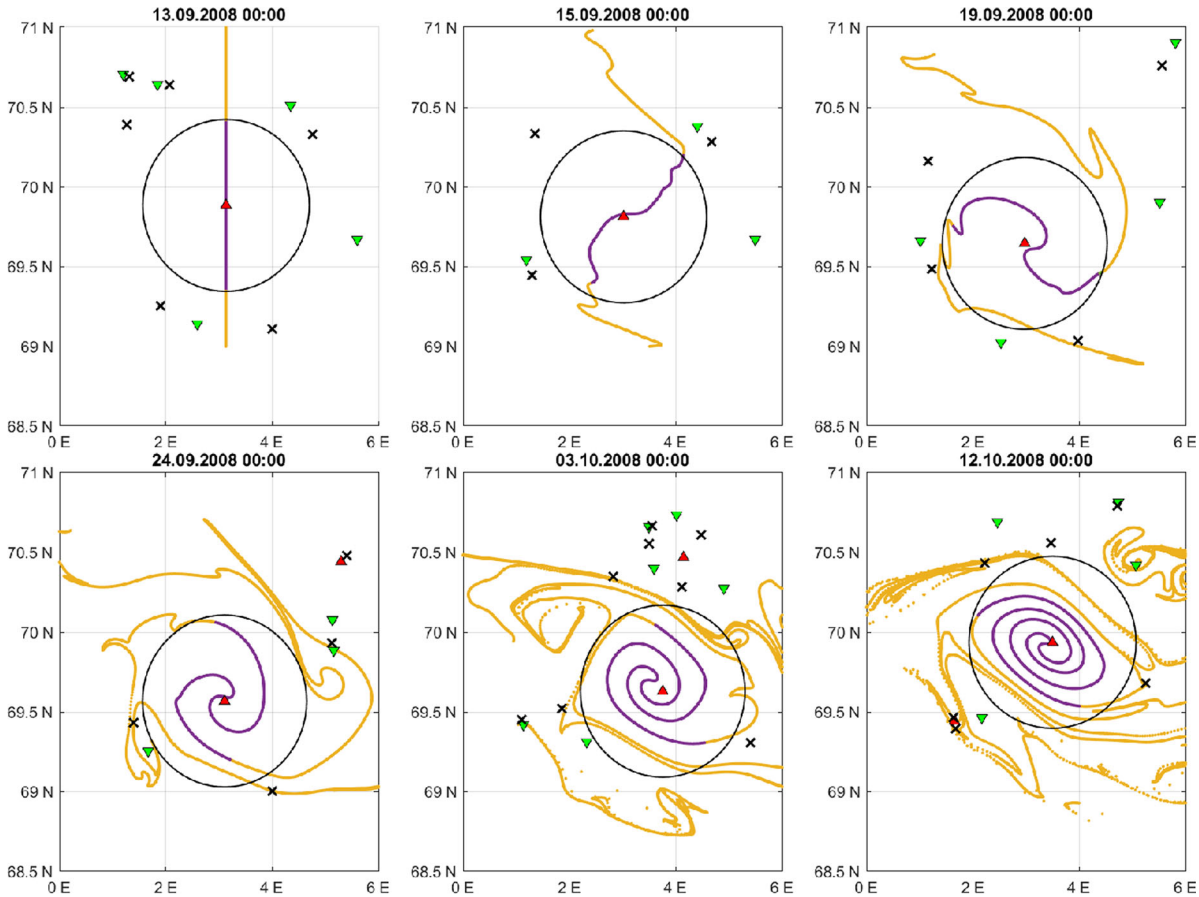

Figure 8
"Experiment with a Circle". The marker spot on the layer of 50 m for the Circle with a radius of 60 km; the evolution of the Segment inside the Circle during the anticyclonic rotation of the Lofoten Vortex. The purple color shows markers of the Segment that are inside the Circle and have not gone beyond it yet; the markers outside the Circle as well, and the markers that replaced the purple markers inside the Circle are shown yellow. The red triangles indicate the centers of anticyclones, and the green ones indicate the centers of cyclones. The crosses show hyperbolic points

stratified in salinity. The resulting density stratification is stable, but the seasonal pycnocline above the center of the LV is about twice as thin (50–70 m) as at its periphery (Bashmachnikov et al., 2017). Isolines of temperature and salinity in the upper layers coincide, but according to ROMS data, the values decrease faster, so the vertical scale of the lens according to GLORYS12V1 (NEMO) data slightly exceeds that according to the ROMS model. However, the horizontal scales of the LV core are the same in both datasets.

The above comparisons confirm the possibility of this ROMS implementation to reproduce the observational features of the thermohaline structure of the LV. A fundamental requirement for the model is a high spatial resolution.

4. *Lagrangian Modeling of the Lofoten Vortex Structure: "Experiment with a Segment"*

In this section, we apply an arsenal of methods developed within the framework of nonlinear geophysical hydrodynamics, which works with both analytically specified velocity fields and flow velocity fields calculated from hydrodynamic models, or

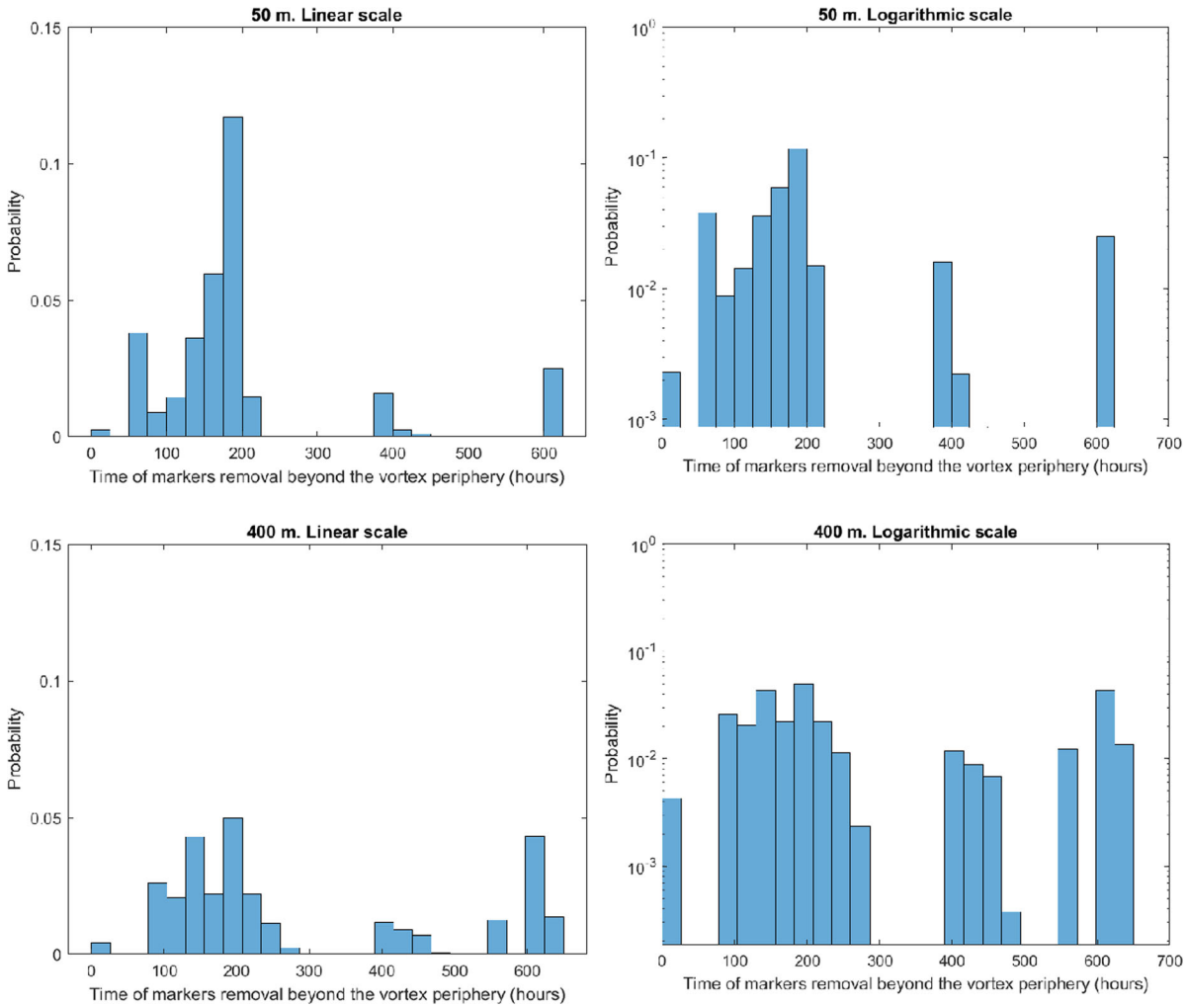

Figure 9
Histograms of the distribution over the time of the removal of markers outside the core of the LV during its evolution at the layers of 50 m and 400 m. Calculations are presented for a radius of 60 km. The values are normalized to the total number of markers on the Segment inside the circle at the initial time

geostrophic flow fields calculated from satellite altimetric data. The Lagrangian approach is useful for determining the 2D structure of vortices, their nuclei, boundaries, and the paths along which they receive and release water (Koshel & Prants, 2006). For Lagrangian analysis of the waters movement, a sufficiently large number of artificial (virtual) particles (markers) are placed in the study area on the surface or one of the horizons, and then advection equations are solved, allowing them to track their trajectories:

$$\frac{d\lambda}{dt} = u(\lambda, \varphi, t), \frac{d\varphi}{dt} = (\lambda, \varphi, t). \quad (1)$$

where u and v are the angular zonal and meridional components of the flow velocity, φ and λ are the latitude and longitude. Angular velocities are used because the equations for them have the simplest possible form on the Earth's sphere. To obtain accurate numerical results, bicubic spatial interpolation and smoothing of time evolution using Lagrange polynomials of the third order are used. Lagrangian

trajectories are calculated by integrating Eq. (1) according to the fourth-order Runge–Kutta scheme with a constant time step of 0.001 days.

The analysis is performed using mapping in geographical coordinates of two Lagrangian indicators: the Lyapunov exponent accumulated over a finite time (Finite Time Lyapunov Exponent, FTLE—Λ-map), and the length of trajectories in a certain time interval (*S*-map) (Prants et al., 2017). The Lagrangian technique used seems to be more suitable for vortex identification than other methods, because FTLE, like trajectory length maps, contain accumulated information about the "history" of waters involved in vortex motion. This fundamentally distinguishes them from such Eulerian characteristics as, for example, relative vorticity or the Okubo-Weiss parameter, which contain useful information but are actually "instantaneous" snapshots at the current time (Novoselova et al., 2024). Therefore, vortices can be seen more clearly on Lagrangian maps than on maps of Eulerian quantities (Fayman et al., 2019; Prants et al., 2013, 2015). The advantage of Lagrangian approaches also lies in the fact that they allow you to "personalize" passive markers, study their trajectories over time, and thereby visualize their movement in a vortex.

In our study, within the framework of the Lagrangian approach, in the period from 00:00 on September 13 to 00:00 on October 13, 2008, every three hours, the area bounded by coordinates 69°–71° N, 1°–6° E, was evenly seeded with Lagrangian particles on a grid of 300 × 300 nodes. Then, for each particle, its trajectory was calculated 5 days ago in time. The basis for particle tracking is the 3D implementation of ROMS, from which we consider the velocity fields of currents on two horizons: 50 m and 400 m. The choice of horizons is due to simple considerations to obtain a representative representation of the LV on their basis: 50 m is the upper quasi-homogeneous layer, and 400 m is the middle of the LV core in depth. The LV core is usually located in a layer from 200 to 800 m (Novoselova, 2022; Travkin & Belonenko, 2021; Trodahl et al., 2020; Volkov et al., 2013, 2015; Yu et al., 2017; Zhmur et al., 2022, and references herein). The choice of the period of the study is also not accidental: in September, the LV lens is well formed and separated from surface waters by a seasonal pycnocline.

By integrating the equations of motion (1) forward or backward in time, we can study the evolution (forward in time) or history (backward in time) of the observed waters. Figure 6 shows the S-maps constructed within the framework of the Lagrangian approach based on both ROMS and AVISO data. The value of the indicator S is equal to the number of kilometers that the Lagrangian particles traveled during the previous five days. S is the length of the trajectory with initial conditions at a given point, integrated back in time by 5 days. The trajectory starts 5 days ago and arrives at the point indicated on the map after 5 days. The Lyapunov exponent is calculated similarly. Figure 6 shows that, according to the results of the ROMS simulation, in areas with intense dynamics, including in the area of the LV location, particles travel more than 100 km in 5 days. Similar calculations of the S indicator were carried out according to AVISO data. These calculations showed that the path that particles travel in the LV region can indeed be 100 km in 5 days. Figure 6 (right column) shows that the configuration of the areas with maximum speeds coincides with the configuration of the areas with the highest values of S on the maps. The yellow line shows a fragment of the marker spot evolution from the "Experiment with a Segment", which will be discussed further.

To determine in which places of the study area the waters movement was regular and in which chaotic, the Lyapunov exponent Λ is calculated. The results of calculations of the Lyapunov exponent Λ for the previous five days are shown in Fig. 7, which shows slides for consecutive time points on September 14, 17, 19, and October 4, 2008. These slides show the evolution of LV in the fields of the Lagrangian indicators Λ and S, as well as the flow velocities.

The key part of the study is the so-called "Experiment with a Segment", which consists of the following. At the initial moment (September 13, 2008, 00:00 h) in the considered water area, meridional segments with coordinates 69°–71° N, 3.1319° E are set at layers of 50 and 400 m passing through the center of the LV and consisting of 100,000 Lagrangian particles shown in yellow in Fig. 7. During the evolution and rotation of the vortex over

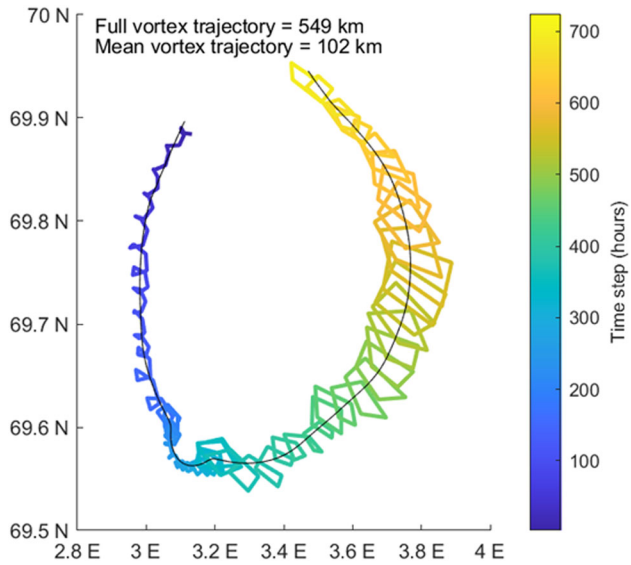

Figure 10
The drift trajectory of the LV center at the layer of 50 m, depending on time

the next 720 h, straight segments deformed into curved lines with the formation of numerous folds, swirls, and curls. This is how chaotic advection manifests itself on the periphery of the LV (Fayman et al., 2019; Prants, 2014; Prants et al., 2013). The slides in Fig. 7 are a visualization of 2D chaotic advection on a layer of 50 m. The "Experiment with a Segment" clearly shows that rotation in vortices is not circular or uniform and similar to rotation of a vinyl record on a music player. The spots of particles previously representing a meridional segment and located in the core of the anticyclone rotate with an angular velocity depending on the distance to the core center. This leads to the formation of a characteristic double helix in the vortex center. The spots of particles located on the periphery of the vortex break away from the rotating core and form many folds, swirls, and curls. The analysis of the slides also allows us to conclude that the hyperbolic points closest to the vortex (shown with crosses) contribute to the extraction of particles portions from the vortex (Prants et al., 2017).

5. *"Experiment with a Circle": Statistics of Particles Leaving the LV Periphery*

At the next stage, we studied the process of particles leaving the LV periphery. The basis for these experiments was the flow velocities calculated in the ROMS model. Recall that in the experiment, these particles were launched on meridional segments on September 13, 2008. We considered these segments at two layers of 50 and 400 m. We surrounded the vortex centers with circles with radii of 30, 40, 50, and 60 km. The centers of the selected circles coincided with the current position of the vortex center at the layer (50 or 400 m). At each moment of experiment time, the center of the circle corresponds to the center of the LV. In Fig. 8, the center of the LV is shown as a red triangle. Next, the time of the first touch of the circle boundary with markers was determined. Markers touching the circle were excluded from further consideration.

Then we estimated the number of markers that intersect the circle during the vortex evolution. Figure 8 shows that the purple spot of markers touches the circle at some point and then crosses it, as a result of which a portion of markers passes into the external

environment, and markers from the external environment come in their place. This means that the exclusion of markers from the circle does not occur gradually, one by one, but in portions. Over time, as can be seen in Fig. 8, the number of purple markers simulating the LV core at the initial moment gradually becomes smaller and smaller, and inside the circle, they are replaced by markers from the external environment. This experiment demonstrates how the vortex exchanges water with the external environment. The complete time series of figures (from September 13 to October 12, 2008) is provided in the supplementary material (S1).

Next, we calculated the number of markers dropping out of the circle depending on time. The graphs in Fig. 9 also show the proportionality of reducing the number of markers inside the circle. It can be seen that during the evolution of the vortex, there are time intervals at which almost all markers remain inside the circle. These intervals can be several days. Similar calculations for the radii of circles of 30, 40, and 50 km are not given in this paper, although the statistics for them differ.

Perhaps the portioning observed during the water exchange of particles of the vortex core and periphery with the environment is because the LV center, which rotates anticyclonically, performs sawtooth horizontal movements with a common trajectory of movement around the circle in the cyclonic direction (Fig. 10). The amplitude of horizontal movements of the LV center is maximal in the eastern part of its location and gradually decreases to the west. The length of the smoothed vortex trajectory is 102 km, and the length of the trajectory, taking into account horizontal fluctuations, is 549 km. The average velocity of the vortex drift is 3.8 cm/s. If we consider all the sawtooth oscillations during drift, the total velocity of the vortex reaches 20 cm/s.

6. *Discussion and Conclusions*

Modern hydrodynamic models of ocean circulation with high spatial resolution have reached a level where their results can significantly complement field observations to obtain a more holistic picture of the evolution of oceanological processes in time and space. The Eulerian approach is most popular in the analysis of hydrodynamic model data, which is explained by the well-established practice of analyzing temperature, salinity, and other parameters at horizontal layers or vertical sections. Creating a three-dimensional vortex model is a kind of Eulerian approach (Sandalyuk et al., 2020).

The Lagrangian approach, when the movement of a specific portion of water is continuously monitored, is indispensable for clarifying the origin and "fate" of particles of water masses. It allows you to solve problems that cannot be solved within the framework of the Eulerian approach. This method provides a unique opportunity to trace the trajectories of the of water masses movement, which is especially important for studying the processes of mixing, particle transportation, and water exchange between different areas. Thanks to this, it is possible to gain a more detailed understanding of the dynamics of the ocean and the interaction of its various components.

For the Lofoten Basin, the Lagrangian approach has previously been successfully applied to solve various problems related to water circulation in this region. So, Fedorov et al. (2021) used this method to identify the origin of waters in the LV core, Belonenko et al. (2021a, 2021b) investigated the formation of a cyclone satellite in the vicinity of the LV, and Travkin et al. (2022), using Lagrangian modeling, discovered a mushroom-shaped dipole of topographic origin in the basin.

In this paper, we also apply the Lagrangian approach, which is based on the high-resolution ROMS model implemented for the Lofoten Basin. Using standard verification and validation methods, we established the representativeness of the ROMS implementation for the period September–October 2008. The obtained flow velocity fields with high spatial resolution were the basis for the application of Lagrangian approaches. For the analysis, we used two Lagrangian indicators: the Lyapunov exponent for finite time (Λ) and the length of the trajectories (S).

We seeded the study area with a large number of virtual particles (Lagrangian markers) and then tracked their evolution over time. We have established that particles in the vortex core and on its periphery have different "destinies": particles in the core located closer to the vortex center move along

closed trajectories with an angular velocity depending on the distance to the center of the vortex. The particles that are located on the periphery, also participating to some extent in the general anticyclonic rotation of the vortex, behave completely differently: they form many folds and swirls of bizarre shapes, entering and exiting the vortex. We call this process "ventilation of the vortex periphery". The formation of folds, swirls, and curls on the spots of these particles is influenced by hyperbolic points located in the immediate vicinity, which can be seen e.g. in Fig. 8.

The setting of the "Experiment with a Segment" for the LV and the conclusions obtained as a result of this analysis constitute the novelty of this work. This experiment allows us to understand how water exchange occurs between the vortex and the environment.

A very important result, which has not been noticed by anyone before, concerns the portioning observed during the exchange of vortex particles with the environment. It turned out that in this process, the particles of the vortex leave it not gradually, one by one, but in portions.

Another interesting result is the oscillatory movements of the LV in the horizontal direction. The LV, as a whole, moves in a cyclonic direction along a circular trajectory with a radius of about 18 km. Note that the amplitude of the oscillations in the eastern part of this circle significantly exceeds the amplitude in the western part. Perhaps this is due to the influence of the bottom topography, in which the movement of the vortex to the west on the eastern flank of the circle develops with a beta effect and is opposite in sign on the western one (LeBlond & Mysak, 1977). The fact of the LV drift in the cyclonic direction was recorded earlier according to field data (Ivanov & Korablev, 1995), the results obtained by us confirm this conclusion. However, our analysis clarifies that the LV not only moves along a cyclic trajectory but also performs horizontal sawtooth oscillations. The average velocity of the vortex drift is 3–4 cm/s, which is slightly higher than the average drift velocity of 1.2 cm/s established in Ivanov and Korablev (1995). However, the empirical velocities based on the oceanographic surveys belong to another period and are obtained with a large error, nevertheless, coinciding in order with our results. Ivanov and Korablev (1995) allow values of the vortex drift velocity in a wide range and up to 8 cm/s.

Author Contributions N.E. is responsible for particle tracking modeling, data analysis and preparing the figures; F.P. is responsible for ocean modeling, data analysis, writing; D.A. is responsible for preparing the figures; B.M. is responsible for 2D Lagrangian modeling; S.I. is responsible for data analysis; B.T. is responsible for literature review and first draft writing; U.M. is responsible for conceptualization. All authors reviewed the manuscript.

Funding

The simulation in ROMS model was carried out with the support of St. Petersburg University grant No. 116442164. The 3D modeling of Lagrangian markers trajectories and statistical analysis of particle removal from the vortex was carried out with the support of Russian Science Foundation grant No. 24-77-00063, https://rscf.ru/project/24-77-00063/. The Lagrangian analysis were made on the high-performance computing cluster at the Pacific Oceanological Institute (State Task No. 124022100072–5) and Shared Resource Center "Far Eastern Computing Resource" IACP FEB RAS (https://cc.dvo.ru).

Data Availability

No datasets were generated or analysed during the current study.

Declarations

Conflict of interest The authors declare that they have no conflict of interest.

Appendix

See Fig. 11.

Table 1

Coordinates and dates of CTD stations

Экспедиция 1987 года				Экспедиция 1989 года				Экспедиция 1990 года			
№	Lon	Lat	Date	№	Lon	Lat	Date	№	Lon	Lat	Date
1	6.5	69	1987-Sep-5	1	0.5	71.5	1989-Sep-10	1	0.5	71.5	1990-Sep-4
2	5	69	1987-Sep-5	2	2	71.5	1989-Sep-10	2	2	71.5	1990-Sep-4
3	3.5	69	1987-Sep-5	3	3.5	71.5	1989-Sep-10	3	3.5	71.5	1990-Sep-4
4	2	69	1987-Sep-5	4	5	71.5	1989-Sep-10	4	5	71.5	1990-Sep-4
5	0.5	69	1987-Sep-5	5	6.5	71.5	1989-Sep-11	5	6.5	71.5	1990-Sep-4
6	0.5	69.5	1987-Sep-6	6	6.5	71	1989-Sep-11	6	6.5	71	1990-Sep-5
7	2	69.5	1987-Sep-6	7	5	71	1989-Sep-11	7	5	71	1990-Sep-5
8	3.5	69.5	1987-Sep-6	8	3.5	71	1989-Sep-12	8	3.5	71	1990-Sep-5
9	5	69.5	1987-Sep-6	9	2	71	1989-Sep-12	9	2	71	1990-Sep-5
10	6.5	69.5	1987-Sep-6	10	0.5	71	1989-Sep-12	10	0.5	71	1990-Sep-6
11	6.5	70	1987-Sep-7	11	0.5	70.5	1989-Sep-12	11	0.5	70.5	1990-Sep-6
12	5	70	1987-Sep-7	12	2	70.5	1989-Sep-13	12	2	70.5	1990-Sep-6
13	3.5	70	1987-Sep-7	13	3.5	70.5	1989-Sep-13	13	3.5	70.5	1990-Sep-6
14	2	70	1987-Sep-7	14	5	70.5	1989-Sep-13	14	5	70.5	1990-Sep-7
15	0.5	70	1987-Sep-7	15	6.5	70.5	1989-Sep-13	15	6.5	70.5	1990-Sep-7
16	0.5	70.5	1987-Sep-8	16	6.5	70	1989-Sep-14	16	6.5	70	1990-Sep-7
17	2	70.5	1987-Sep-8	17	5	70	1989-Sep-14	17	5	70	1990-Sep-8
18	3.5	70.5	1987-Sep-8	18	3.5	70	1989-Sep-14	18	3.5	70	1990-Sep-8
19	5	70.5	1987-Sep-8	19	2	70	1989-Sep-14	19	2	70	1990-Sep-8
20	6.5	70.5	1987-Sep-8	20	0.5	70	1989-Sep-14	20	0.5	70	1990-Sep-8
21	6.5	71	1987-Sep-9	21	0.5	69.5	1989-Sep-15	21	0.5	69.5	1990-Sep-9
22	5	71	1987-Sep-9	22	2	69.5	1989-Sep-15	22	2	69.5	1990-Sep-9
23	3.5	71	1987-Sep-9	23	3.5	69.5	1989-Sep-15	23	3.5	69.5	1990-Sep-9
24	2	71	1987-Sep-9	24	5	69.5	1989-Sep-15	24	5	69.5	1990-Sep-9
25	0.5	71	1987-Sep-9	25	6.5	69.5	1989-Sep-16	25	6.5	69.5	1990-Sep-9
				26	6.5	69	1989-Sep-16	26	6.5	69	1990-Sep-10
				27	5	69	1989-Sep-16	27	5	69	1990-Sep-10
				28	3.5	69	1989-Sep-17	28	3.5	69	1990-Sep-11
				29	2	69	1989-Sep-17	29	2	69	1990-Sep-11
				30	0.5	69	1989-Sep-17	30	0.5	69	1990-Sep-11
				31	0.5	68.5	1989-Sep-18	31	0.5	68.5	1990-Sep-12
				32	2	68.5	1989-Sep-18	32	2	68.5	1990-Sep-12
				33	3.5	68.5	1989-Sep-18	33	3.5	68.5	1990-Sep-12
				34	5	68.5	1989-Sep-18	34	5	68.5	1990-Sep-12
				35	6.5	68.5	1989-Sep-18	35	6.5	68.5	1990-Sep-12

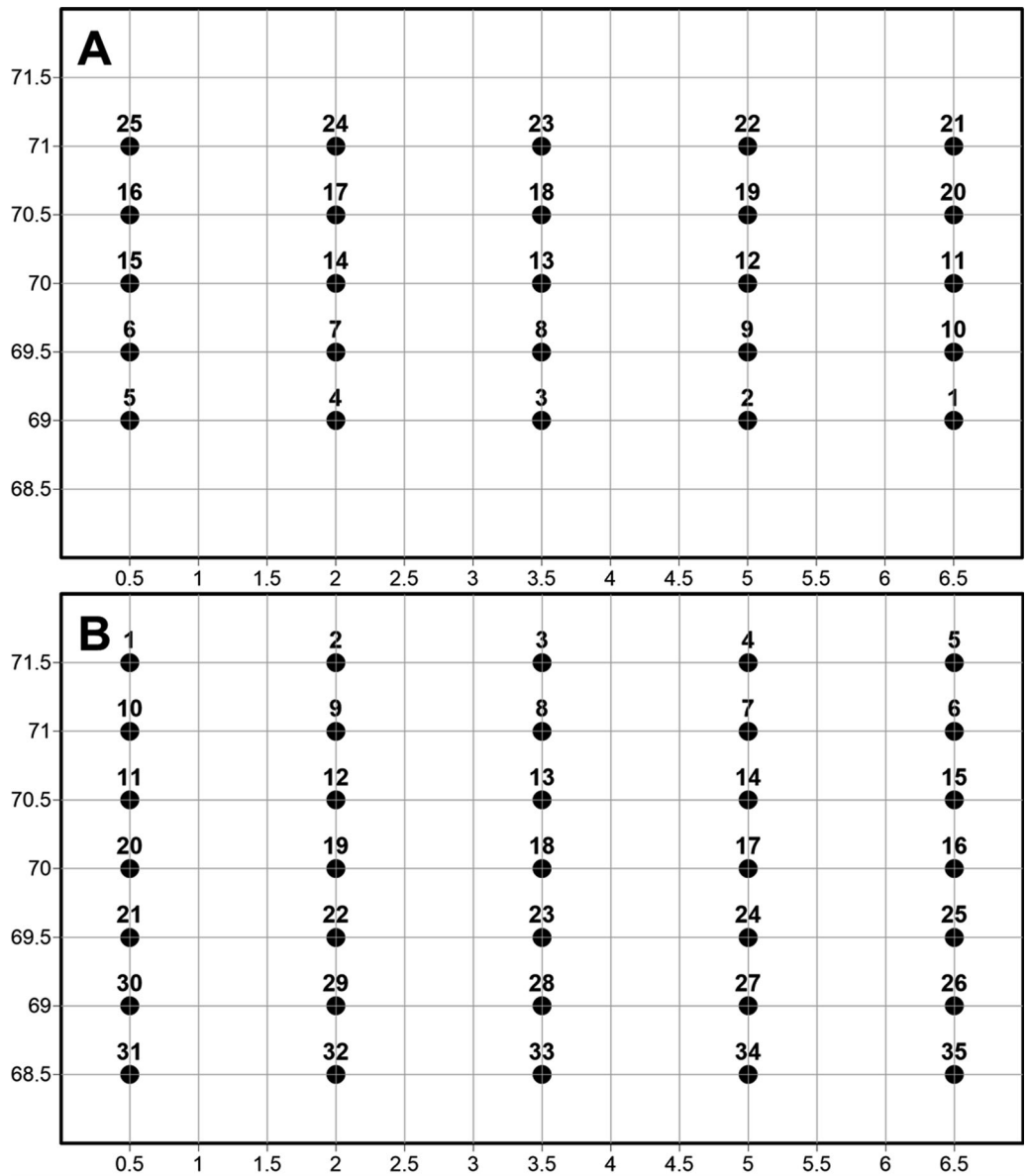

Figure 11
Diagram of CTD stations in the September 1987 expedition (**A**) and the September 1989 and 1990 expeditions (**B**)

by the terms of such publishing agreement and applicable law.

References

Bashmachnikov, I., Sokolovskiy, M. A., Belonenko, T. V., Volkov, D. L., Isachsen, P. E., & Carton, X. (2017). On the vertical structure and stability of the Lofoten vortex in the Norwegian Sea. *Deep-Sea Research Part I, 128*, 1–27. https://doi.org/10.1016/j.dsr.2017.08.001

Belonenko, T. V., Travkin, V. S., Koldunov, A. V., & Volkov, D. L. (2021a). Topographic experiments over dynamical processes in the Norwegian Sea. *Russian Journal of Earth Sciences, 21*, ES1006. https://doi.org/10.2205/2020ES000747

Belonenko, T. V., Volkov, D. L., Norden, Yu. E., & Ozhigin, V. K. (2014). Water circulation in the Lofoten Basin of the Norwegian Sea. *Vestn s. Petersbur. Un-Ta, Ser.7, 2*, 108–121. in Russian.

Belonenko, T. V., Zinchenko, V. A., Fedorov, A. M., Budyansky, M. V., Prants, S. V., & Uleysky, MYu. (2021b). Interaction of the Lofoten Vortex with a satellite cyclone. *Pure and Applied Geophysics, 178*, 287–300. https://doi.org/10.1007/s00024-020-02647-1

Bentamy, A., & Croize Fillon, D. (2012). Gridded surface wind fields from Metop/ASCAT measurements. *International Journal of Remote Sensing, 33*, 1729–1754. https://doi.org/10.1080/01431161.2011.600348

Blindheim, J., & Østerhus, S. (2013). The Nordic Seas, main oceanographic features. *Geophysical Monograph Series,* 11–37. https://doi.org/10.1029/158GM03

Boyer, T. P., Baranova, O. K., Coleman, C., Garcia, H. E., Grodsky, A., Locarnini, R. A., Mishonov, A. V., Paver, C. R., Reagan, J. R., Seidov, D., Smolyar, I. V., Weathers, K., & Zweng, M. M. (2018). World ocean database 2018. A.V. Mishonov, Technical Ed., NOAA Atlas NESDIS 87. https://www.ncei.noaa.gov/sites/default/files/2020-04/wod_intro_0.pdf

Carton, X. (2001). Hydrodynamical modeling of oceanic vortices. *Surveys in Geophysics, 22*, 179–263.

Cushman-Roisin, B. (1994). *Introduction to geophysical fluid dynamics*. Prentice-Hall.

Fayman, P. A. (2015). Seasonal variability of the circulation of the waters of the Sea of Okhotsk, calculated on the basis of a stationary ocean model. *Vestnik of Far Eastern Branch of Russian Academy of Sciences, 6*(184), 21–28. in Russian.

Fayman, P. A., & Ponomarev, V. I. (2018). Diagnostic calculations of the circulation of the waters of Peter the Great Bay according to the data of the DVNIGMI expedition 2007–2010. *Bulletin of the Far Eastern Branch of the Russian Academy of Sciences, 1*(197), 60–70. in Russian.

Fayman, P. A., Prants, S. V., Budyansky, M. V., & Uleysky, MYu. (2019). Coastal summer eddies in the Peter the Great Bay of the Japan sea: In situ data, numerical modeling and Lagrangian analysis. *Continental Shelf Research, 181*, 143–155. https://doi.org/10.1016/j.csr.2019.05.002

Fedorov, A. M., Belonenko, T. V., Budyansky, M. V., Prants, S. V., Uleysky, MYu., & Bashmachnikov, I. L. (2021). Lagrangian modelling of water circulation in the Lofoten Basin. *Dynamics of Atmospheres and Oceans, 96*, 101258. https://doi.org/10.1016/j.dynatmoce.2021.101258

Good, S., Fiedler, E., Mao, C., Martin, M. J., Maycock, A., Reid, R., Roberts-Jones, J., Searle, T., Waters, J., While, J., & Worsfold, M. (2020). The current configuration of the OSTIA system for operational production of foundation sea surface temperature and ice concentration analyses. *Remote Sensing, 12*, 720. https://doi.org/10.3390/rs12040720

Ivanov, V. V., & Korablev, A. A. (1995). Dynamics of an intrapycnocline lens in the Norwegian Sea. *Russian Meteorology and Hydrology, 10*, 32–37. in Russian.

Kanamitsu, M., Ebisuzaki, W., Woollen, J., Yang, S. K., Hnilo, J. J., Fiorino, M., & Potter, G. L. (2002). NCEP-DOE AMIP-II reanalysis (R-2). *Bulletin of the American Meteorological Society, 83*, 1631–1643. https://doi.org/10.1175/bams-83-11-1631

Kennelly, M. A., Evans, R. H., & Joyce, T. M. (1985). Small-scale cyclones on the periphery of Gulf Stream warm-core rings. *Journal of Geophysical Research, 90*(C5), 8845–8857.

Kochergin, V. P. (1978). *Theory and methods of calculation of oceanic currents*. Nauka. in Russian.

Koldunov, A. V., & Belonenko, T. V. (2020). Hydrodynamic modeling of vertical velocities in the Lofoten vortex. *Izvestiya, Atmospheric and Oceanic Physics, 56*(5), 502–511. https://doi.org/10.1134/S0001433820040040

Koshel, K. V., & Prants, S. V. (2006). Chaotic advection in the ocean. *Physics-Uspekhi, 49*(11), 1151–1178. https://doi.org/10.1070/PU2006v049n11ABEH006066

LeBlond, P., & Mysak, L. A. (1977). *Waves in the ocean*. Elsevier Scientific Publishing Company.

Lellouche, J.-M., Greiner, E., Le Galloudec, O., Garric, G., Regnier, C., Drevillon, M., et al. (2018). Recent updates on the copernicus marine service global ocean monitoring and forecasting real-time 1/12° high resolution system. *Ocean Science, 14*, 1093–1126. https://doi.org/10.5194/os-14-1093-2018

NOAA National Geophysical Data Center. (2006). 2-minute gridded global relief data (ETOPO2) v2. NOAA National Centers for Environmental Information. https://doi.org/10.7289/V5J1012Q

Novoselova, E. V. (2022). Seasonal variability of the potential vorticity in the Lofoten vortex. *Russian Journal of Earth Sciences, 22*(3), ES3006. https://doi.org/10.2205/2022ES000786

Novoselova, E. V., Travkin, V. S., Lebedeva, M. A., Udalov, A. A., Budyansky, M. V., & Belonenko, T. V. (2024). Features of the vortex structures in the fields of Eulerian and Lagrangian hydrological characteristics for the Northwest Pacific. *Vestnik of Saint Petersburg University. Earth Sciences*. https://doi.org/10.21638/spbu07.2024.209

Prants, S. V. (2014). Chaotic Lagrangian transport and mixing in the ocean. *The European Physical Journal Special Topics, 223*(13), 2723–2743. https://doi.org/10.1140/epjst/e2014-02288-5

Prants, S. V., Ponomarev, V. I., Budyansky, M. V., Uleysky, MYu., & Fayman, P. A. (2013). Lagrangian analysis of mixing and transport of water masses in the marine bays. *Izvestiya, Atmospheric and Oceanic Physics, 49*(1), 82–96. https://doi.org/10.1134/S0001433813010088

Prants, S. V., Ponomarev, V. I., Budyansky, M. V., Uleysky, MYu., & Fayman, P. A. (2015). Lagrangian analysis of the vertical structure of eddies simulated in the Japan Basin of the Japan/East Sea. *Ocean Modelling, 86*, 128–140. https://doi.org/10.1016/j.ocemod.2014.12.010

Prants, S. V., Uleysky, MYu., & Budyansky, M. V. (2017). *Lagrangian oceanography: Large-scale transport and mixing in the ocean. Physics of earth and space environments*. Springer.

Pujol, M.-I., Faugère, Y., Taburet, G., Dupuy, S., Pelloquin, C., Ablain, M., & Picot, N. (2016). DUACS DT2014: The new multi-mission altimeter dataset reprocessed over 20 years. *Ocean Science., 12*, 1067–1090.

Reagan, J. R., Garcia, H. E., Boyer, T. P., Baranova, O. K., Bouchard, C., Cross, S. L., Dukhovskoy, D., Grodsky, A., Locarnini, R. A., Mishonov, A. V., Paver, C. R., Seidov, D., & Wang Z. (2024). *World Ocean Atlas 2023*. NOAA National Centers for Environmental Information. Dataset: NCEI Accession 0270533.

Ryzhov, E. A., & Koshel', K. V. (2011). Ventilation of a trapped topographic eddy by a captured free eddy. *Izvestiya, Atmospheric and Oceanic Physics, 47*(6), 780–791.

Sandalyuk, N. V., Bosse, A., & Belonenko, T. V. (2020). The 3D structure of Mesoscale Eddies in the Lofoten Basin of the Norwegian Sea: A composite analysis from altimetry and in situ data. *Journal of Geophysical Research: Oceans, 125*, e2020JC016331. https://doi.org/10.1029/2020JC016331

Santeva, E. K., Bashmachnikov, I. L., & Sokolovskiy, M. A. (2021). On the stability of the Lofoten vortex in the Norwegian Sea. *Oceanology, 61*(3), 308–318. https://doi.org/10.1134/S0001437021030127

Sarkisyan, A. S. (1977). *Numerical analysis and forecast of sea currents*. Hydrometeoizdat. in Russian.

Shchepetkin, A. F. (2003). A method for computing horizontal pressure-gradient force in an oceanic model with a nonaligned vertical coordinate. *Journal of Geophysical Research, 108*(C3), 3090. https://doi.org/10.1029/2001JC001047

Shchepetkin, A. F., & McWilliams, J. C. (2005). The regional oceanic modeling system (ROMS): A split-explicit, free-surface, topography-following-coordinate oceanic model. *Ocean Modelling, 9*(4), 347–404. https://doi.org/10.1016/j.ocemod.2004.08.002

Sokolovskiy, M. A. (1988). Numerical modeling of nonlinear instability for axisymmetric two-layer vortices. *Izvestiya, Atmospheric and Oceanic Physics, 24*(7), 536–542.

Stewart, R. H. (2006). *Introduction to physical oceanography*. Department of Oceanography, Texas A&M University.

Travkin, V. S., & Belonenko, T. V. (2021). Study of the mechanisms of vortex variability in the lofoten basin based on energy analysis. *Physical Oceanography, 28*(3), 294–308. https://doi.org/10.22449/1573-160X-2021-3-294-308

Travkin, V. S., Belonenko, T. V., Budyansky, M. V., Uleysky, MYu., Gnevyshev, V. G., & Raj, R. P. (2022). Quasi-permanent mushroom-like dipole in the Lofoten Basin. *Pure and Applied Geophysics, 179*(1), 465–482. https://doi.org/10.1007/s00024-021-02922-9

Trodahl, M., Isachsen, P. E., Lilly, J. M., Nilsson, J., & Nils, M. K. (2020). The regeneration of the Lofoten vortex through vertical alignment. *Journal of Physical Oceanography, 50*(9), 2689–2711. https://doi.org/10.1175/JPO-D-20-0029.1

Volkov, D. L., Belonenko, T. V., & Foux, V. R. (2013). Puzzling over the dynamics of the Lofoten Basin—A sub-Arctic hot spot of ocean variability. *Geophysical Research Letters, 40*(4), 738–743. https://doi.org/10.1002/grl.50126

Volkov, D. L., Kubryakov, A., & Lumpkin, R. (2015). Formation and variability of the Lofoten Basin vortex in a high-resolution ocean model. *Deep Sea Research I, 105*, 142–157. https://doi.org/10.1016/j.dsr.2015.09.001

Yu, L.-S., Bosse, A., Fer, I., Orvik, K. A., Bruvik, E. M., Hessevik, I., & Kvalsund, K. (2017). The Lofoten Basin eddy: Three years of evolution as observed by Seagliders. *Journal of Geophysical Research: Oceans, 122*, 6814–6834. https://doi.org/10.1002/2017JC012982

Zhmur, V. V. (2011). *Mesoscale vortices of the ocean*. GEOS. in Russian.

Zhmur, V. V., Belonenko, T. V., Novoselova, E. V., & Suetin, B. P. (2023). Conditions for transformation of a mesoscale vortex into a submesoscale vortex filament when the vortex is stretched by an inhomogeneous barotropic flow. *Oceanology, 63*(2), 174–183. https://doi.org/10.1134/S0001437023020145

Zhmur, V. V., Novoselova, E. V., & Belonenko, T. V. (2022). Peculiarities of formation the of density field in mesoscale eddies of the Lofoten Basin: Part 2. *Oceanology, 62*(3), 289–302. https://doi.org/10.1134/S0001437022030171

Zweng, M., Reagan, J., Seidov, D., Boyer, T., Locarnini, R., Garcia, H., Mishonov, A., Baranova, O., Weathers, K., Paver, C., & Smolyar, I. (2019). World ocean atlas 2018, Volume 2: Salinity. A. Mishonov, Technical Editor, NOAA Atlas NESDIS 82.

(Received September 28, 2024, revised November 5, 2024, accepted November 8, 2024, Published online November 27, 2024)